Enhanced Corrosion Prevention Effect of Polysulfone–Clay Nanocomposite Materials Prepared by Solution Dispersion

Jui-Ming Yeh,[1] Chi-Lun Chen,[1] Yen-Chen Chen,[1] Chin-Yi Ma,[1] Hsi-Ya Huang,[1] Yuan-Hsiang Yu[2]

[1]*Department of Chemistry and Center for Nanotechnology at CYCU, Chung-Yuan Christian University, Chung Li, Taiwan 320, China*
[2]*Department of Electronic Engineering, Lan-Yan Institute of Technology, I-Lan 261, Taiwan, China*

Received 24 March 2003; accepted 20 June 2003

ABSTRACT: A series of polymer–clay nanocomposite (PCN) materials containing polysulfone (PSF) and layered MMT clay were successfully prepared by effectively dispersing inorganic nanolayers of MMT clay in an organic PSF matrix via a solution dispersion technique. The synthesized PCN materials were subsequently investigated with a series of characterization techniques, including Fourier transform infrared (FTIR) spectroscopy, wide-angle powder X-ray diffraction (XRD) and transmission electron microscopy (TEM). The prepared PCN coatings with low clay loading (1 wt %) on cold-rolled steel (CRS) were found to be superior in corrosion prevention to those of bulk PSF, based on a series of electrochemical measurements of corrosion potential, polarization resistance, corrosion current and electrochemical impedance spectroscopy (EIS) in a 5 wt % aqueous NaCl electrolyte. The effects of material composition on the molecular barrier, mechanical strength and optical clarity of PSF and PCN materials, in the form of membranes, was also studied by molecular permeability analysis (GPA), dynamic mechanical analysis (DMA) and UV-Visible transmission spectra, respectively. © 2004 Wiley Periodicals, Inc. J Appl Polym Sci 92: 631–637, 2004

Key words: nanocomposites; clay; corrosion; impedance; polymer

INTRODUCTION

Many polymers have been found to be successfully reinforced by the introduction of glass fibers or other inorganic materials. In these reinforced composites, the polymer and additive are not homogeneously dispersed on the microscopic level. If the dispersion could be achieved on the nanoscale level, the mechanical properties would be expected to be further improved, and new, unexpected characteristics might appear.[1] Clay mineral is a potential candidate as an inorganic additive because it has layered silicates, 1 nm thick, and can be intercalated with organic molecules.[2] The lack of affinity between hydrophilic silicate and hydrophobic polymers make it difficult to make them homogeneously miscible with each other. Swelling of each template of silicate with organic molecules is a matter of vital importance to achieve this type of molecular composite.

Recently, polymer–clay nanocomposite (PCN) materials have attracted great attention because their unique features give them many potential applications. PCN materials have been reported to boost the thermal,[3] mechanical,[4] molecular barrier[5] and flame retardant[6] properties of polymers at low clay loading. A key discovery in the field can be traced to the 1990 research work on polyamide–clay nanocomposites by Toyota's research group.[7] Numerous PCN systems were effectively developed by the dispersion of alkylammonium-exchanged forms of montmorillonites (MMT) in various polymer matrices, such as polyacrylonitrile,[8] poly(methyl methacrylate),[9] polystyrene,[10] polyimide,[11] epoxy resin,[12] polyurethane,[13] polyaniline,[14] poly(N-vinyl carbazole),[15] polypyrrole,[16] and others.

Corrosion control was a significant subject of interest to the metal finishing industry. Many polymeric coatings had been designed to protect metals from in-service corrosion. The primary effect of a polymeric coating is to function as a physical barrier against aggressive species such as O_2 and H^+. However, polymeric coatings are not permanently impenetrable, and once there are defects in the coatings, pathways will be formed for the corrosive species to attack the metallic substrate, and localized corrosion will occur. MMT clay with a lamellar shape could be experimentally introduced into many conventional polymeric coatings to effectively increase the length of the diffusion pathways for oxygen gas and water vapor as well as to decrease the permeability of the coating as a second line of defense against corrosion. Recently, we found that the introduction of nanolayers of MMT clay into polymeric matrices [e.g. polyaniline,[17] poly(methyl methacrylate),[18] poly(*ortho*-ethoxyaniline)[19]] could effectively enhance the corrosion prevention effect of

Correspondence to: J.-M. Yeh (juiming@cycu.edu.tw).

Journal of Applied Polymer Science, Vol. 92, 631–637 (2004)

bulk polymers on cold-rolled steel in saline under various conditions.

Polysulfone (PSF), a commercially available transparent engineering plastic with good film formation property, is typically used in medical and food-processing equipment, electrical and electronic components, camera cases, and piping.[20] Mark et al.[21] reported the mechanical properties and thermal stability of PSF–clay nanocomposite materials. However, the corrosion prevention properties of PSF–clay nanocomposite materials has never been reported. Therefore, in this article, we focus on the corrosion prevention performance of PSF–clay nanocomposite materials, prepared from solution dispersion, in the form of coatings on metallic surfaces in saline.

The effects of material composition on molecular barrier, mechanical strength and optical clarity of PSF and PCN materials, in the form of membranes, were investigated by molecular permeability analysis, dynamic mechanical analysis and UV-visible transmission spectra, respectively.

EXPERIMENTAL

Chemicals and Instrumentation

PSF (AMOCO, Udel P-3500, Fw = 35,000; Solvay S.A., Belgium), N-methyl-2-pyrrolidone (NMP) (TEDIA, >99%; Fairfield, OH) were used as received without further purification. Dodecylamine (Fluka, ≧98%; Switzerland) was used as the intercalating agent. The MMT clay (Kunipia-F), supplied by Industrial Technology Research Institute (ITRI), had a unit cell formula of $Ca_{0.084}Na_{0.143}(Al_{1.69}Mg_{0.31})Si_4O_{10}\bullet 2H_2O$ and a CEC value of 114 mEq/100 g.

Wide-angle X-ray diffraction study of the samples was performed on a Rigaku D/MAX-3C OD-2988N X-ray diffractometer with a copper target and a Ni filter at a scanning rate of 2°/min. Fourier transform infrared (FTIR) spectra were measured on pressed KBr pellets using a JASCO FT/IR-460 plus spectrometer. The samples for transmission electron microscopy (TEM) study were prepared by putting the membranes of PCN materials into epoxy resin capsules and curing the epoxy capsules at 100°C for 24 h in a vacuum oven. The cured epoxy resin capsules containing PCN materials were then microtomed with a Reichert–Jumg Ultracut-E into 60–90 nm thick slices. Subsequently, one layer of carbon of about 10 nm in thickness was deposited on these slices on mesh 100 copper nets for TEM observations on a JEOL-200FX with an acceleration voltage of 120 kV.

Corrosion potential, polarization resistance, corrosion current and electrochemical impedance spectroscopy were performed on sample-coated cold-rolled steel (CRS) coupons with VoltaLab 21 and VoltaLab 40 Potentiostat/Galvanostat machines in a standard corrosion cell equipped with two graphite rod counter-electrodes and a saturated calomel electrode (SCE) in addition to the working electrode. A Yanagimoto Co., Ltd. gas permeability analyzer (model GTR 10) was used to carry out the permeation experiment of oxygen gas and water vapor. The dynamic mechanical analyses for the prepared membrane samples were carryied out from 20 to 250°C with a Perkin–Elmer DMA 7 serial analyzer at a heating rate of 5°C/min and a fixed frequency of 1 Hz. UV-visible transmission spectra were obtained using a Hitachi U-2000 UV-visible spectrometer.

Preparation of Organophilic Clay

The organophilic clay was prepared by a cationic-exchange reaction between the sodium cations of MMT clay and the alkylammonium ions of the intercalating agent, dodecylamine. The equation to calculate the amount of intercalating agent used for the cationic-exchange reaction is as follows:

$$114/100 \times 5\text{g(MMT)} \times 1.5 = (X/M_w \text{ of intercalating agent}) \times 1 \times 1000 \quad (1)$$

where X is the amount of intercalating agent used, 114/100 represents the CEC value per 100 g of MMT, 1.5 (>1) indicates the excess amount of intercalating agent used. For most formulations, 5 g of MMT clay with a CEC value of 114 mEq/100 g were stirred in 500 mL of distilled water (beaker A) at room temperature overnight. A separate solution containing 1.58 g of intercalating agent in another 100 mL of distilled water (beaker B) was magnetically stirred, and then an aqueous solution of 1.0M HCl was added to adjust the pH value to about 3-4. After stirring for 1 h, the protonated amino acid solution (beaker B) was added at a rate of approximately 10 mL/min with vigorous stirring to the MMT suspension (beaker A). The mixture was stirred overnight at room temperature. The organophilic clay was recovered by ultracentrifuging (9000 rpm, 30 min) and filtering the solution in a Buchner funnel. Purification of products was performed through washing and filtering samples at least five times to remove any excess ammonium ions.

Preparation of PSF–Clay Nanocomposites by Solution Dispersion

First, organophilic clay contents of 1 wt %, 3 wt %, 5 wt %, 7 wt % and 10 wt % with respect to PSF were introduced into NMP under magnetic stirring for 24 h at room temperature. PSF was subsequently added to the previously described organophilic clay solution of NMP to form a 1 wt % of PSF–clay nanocomposite solution with different clay loading. Under vigorous

stirring for an additional 12 h at room temperature, the prepared PSF–clay nanocomposite solution was subsequently filtered with a 0.45 μm hydrophilic PVDF filter (Millpore Millev-HV) and cast onto a glass plate (5 cm × 5 cm, ≈3 cc/pcs) and dried at 40°C for 12 h to yield a membrane of PSF–clay nanocomposite. For example, a 1 wt % PSF–clay nanocomposite solution containing 5 wt % organophilic clay was prepared as follows: 0.0105 g of organophilic clay was dispersed in 20.84 g of NMP under magnetic stirring for 24 h at room temperature. A quantity of 0.2 g of PSF was subsequently introduced into the organophilic clay solution and stirred for an additional 12 h at room temperature to give a PSF–clay nanocomposite solution. This solution was filtered with a 0.45 μm hydrophilic PVDF filter (Millpore Millev-HV) and then cast onto 6 pcs of glass plate (5 cm × 5 cm, ≈3 cc/pcs) for membrane preparation.

Preparation of Coatings and Electrochemical Measurements

PSF and PCN fine powders were dissolved in NMP to give (in most cases) 1 wt % solutions for improving film formation. The solutions were cast dropwise onto CRS coupons (1.0 × 1.0 cm) followed by drying in air for 24 h at 40°C to give coatings of ≈25 μm in thickness, measured by digimatic micrometer (Mitutoyo). The coating ability of PCN onto CRS was similar to that of bulk PSF. The coated and uncoated coupons were then mounted on the working electrode so that only the coated side of the coupon was in direct contact with the electrolyte. The edges of the coupons were sealed with super-fast epoxy cement (SPAR®). All of the electrochemical measurements of corrosion potential, polarization resistance and corrosion current were performed on a VoltaLab model 21 Potentiostat/Galvanostat and repeated at least three times. The electrolyte used was NaCl (5 wt %) aqueous solution. The open circuit potential (OCP) at the equilibrium state of the system was recorded as the corrosion potential (E_{corr} in volts vs. SCE). The polarization resistance (R_p in °/cm^2) was measured by sweeping the applied potential from 20 mV below to 20 mV above the E_{corr} at a scan rate of 500 mV/min and recording the corresponding current change. The R_p value was obtained from the slope of the potential-versus-current plot. The Tafel plots were obtained by scanning potential from 250 mV below to 250 mV above the E_{corr} at a scan rate of 500 mV/min. Corrosion current (i_{corr}) was determined by superimposing a straight line along the linear portion of the cathodic or anodic curve and extrapolating it through E_{corr}. The corrosion rate (R_{corr}, in milli-inches per year, MPY) was calculated from the following equation:

$$R_{corr}(\text{MPY}) = [0.13\, i_{corr}(\text{E.W.})]/[A \cdot d] \qquad (2)$$

where E.W. is the equivalent weight (in g/Eq), A is the area (in cm^2) and d is the density (in g/cm^3).

VoltaLab model 40 Potentiostat/Galvanostat was used to perform the AC impedance spectroscopy measurements. Voltamaster 4 (Version 2.0), supplied by Radiometer Copenhagen, was the software used. Impedance measurements were performed in the frequency range of 100 KHz–100 mHz. The working electrode was first maintained in the test environment for 30 min before the impedance run. The purpose of this step was to standardize the electrodes in a reproducible initial state and to ensure that no blistering occurred during the conditioning period. All experiments were performed at a laboratory temperature of 25 ± 1°C. All raw data were tested at least three times to insure reproducibility and statistical significance.

Preparation of Membranes and Barrier Property Measurements

A 1 wt % PSF and PSF–clay nanocomposite solution prepared by solution dispersion was subsequently cast onto a glass substrate. The solvent was allowed to evaporate at 40°C under the fume hood for 24 h. The as-prepared sample-coated glass substrate was then immersed in water to give PSF–clay nanocomposite membranes.

Oxygen permeability of membrane was determined by using a Yanco GTR-10 gas permeability analyzer. Gas permeability was calculated by the following equation:

$$P = l/(p_1 - p_2) \times \frac{q/t}{A} \qquad (3)$$

where P is the gas permeability [cm^3(STP)-cm/cm^2-s-cmHg], q/t is the volumetric flow rate of gas permeate [cm^3(STP)/s], l is the membrane thickness (cm), A is the effective membrane area (cm^2), and p_1 and p_2 are the pressures (cmHg) on the high pressure and low pressure sides of the membrane, respectively. The rate of transmission of O_2 was obtained by gas chromatography, from which the air permeability was calculated. On the other hand, the experiment of H_2O permeability was performed with the same apparatus, except that the feed solution was not in contact with the membrane. The feed solution was vaporized first and subsequently permeated through a membrane with an effective area of ≈10.2 cm^2. The permeation rate was determined by measuring the weight of permeate.

RESULTS AND DISCUSSION

MMT is a clay mineral containing stacked silicate sheets measuring ≈10 Å in thickness and ≈2180 Å in length.[22] It has a high aspect ratio and a plate-like

TABLE I
Relation of Composition of Polysulfone–MMT Clay Nanocomposite Materials to E_{corr}, R_p, i_{corr}, and R_{corr} Measured by Electrochemical Methods

Compound Code	Feed Composition (wt %)		Electrochemical Corrosion Measurements			
	Polysulfone	MMT	E_{corr} (mV)	R_p (kΩ · cm^2)	i_{corr} (μ A/cm^2)	R_{corr} (MPY)
Blank	—	—	−641	0.8	44.4	20.72
CLSF0	100	0	−600	7.99	7.8768	3.666
CLSF1	99	1	−529.7	32.30	1.7274	0.804
CLSF10	90	10	−363.6	44.09	1.3362	0.622

Saturated calomel electrode was used as reference electrode.

morphology. Typically, the chemical structure of MMT consists of two fused silica tetrahedral sheets sandwiching an edge-shared octahedral sheet of either magnesium or aluminum hydroxide. The Na^+ and Ca^{+2} residing in the interlayer regions can be replaced by organic cations such as alkylammonium ions by a cationic-exchange reaction to render the hydrophilic-layered silicate organophilic. To synthesize the PCN materials, organophilic clay was first successfully prepared by a cationic-exchange reaction between the sodium cations of MMT clay and the alkylammonium ions of the intercalating agent. Organophilic clay was subsequently disperse into the PSF matrix through a solution dispersion technique. The composition of the PCN materials was varied from 0 to 10 wt % of clay with respect to PSF content, as summarized in Table I.

Characterization

The representative FTIR spectra of the organophilic clay, bulk PSF and PCN materials are shown in Figure 1. The characteristic vibration bands of PSF are at 1160 cm^{-1} (symmetric sulfone stretching),[21] 1240 cm^{-1} (aromatic ether), 1328 cm^{-1} (asymmetric sulfone stretching) and 3000≈3100 cm^{-1} (aromatic CH_3 stretching), and 2800≈3000 cm^{-1} (aliphatic CH_3 stretching). Those of MMT clay were shown at 1040 cm^{-1} (Si—O), 523 cm^{-1} (Al—O) and 464 cm^{-1} (Mg—O).[17–19] As the loading of MMT clay increased, the characteristic peaks of MMT clay became sharper in the FTIR spectra of PCN materials. Figure 2 shows the wide-angle powder X-ray diffraction patterns of organophilic clay and a series of PCN materials. For CLSF1, there was a lack of any diffraction peak in 2θ = 2–10° as opposed to the diffraction peak at 2θ = 5.00° (d spacing = 1.76 nm) for organophilic clay, implying the possibility of exfoliated silicate nanolayers of organophilic clay dispersed in the PSF matrix. For CLSF10, there was a small peak appearing at 2θ = 4.10°, corresponding to a d spacing of 2.15 nm. This implies that there is a small amount of organoclay that cannot be exfoliated in the PSF and exists in the form of an intercalated layer structure.

In Figure 3, TEM of PCN materials containing 10 wt % clay (CLSF10) at 50K magnification reveal that the nanocomposite displayed a mixed nanomorphology. Individual silicate layers, along with two and three layer stacks, were found to be exfoliating in the PSF matrix. Some larger intercalated tactoids could also be observed.

Corrosion Prevention Effect of Coatings

The corrosion prevention effect of sample coated CRS coupons can be evaluated by the values of

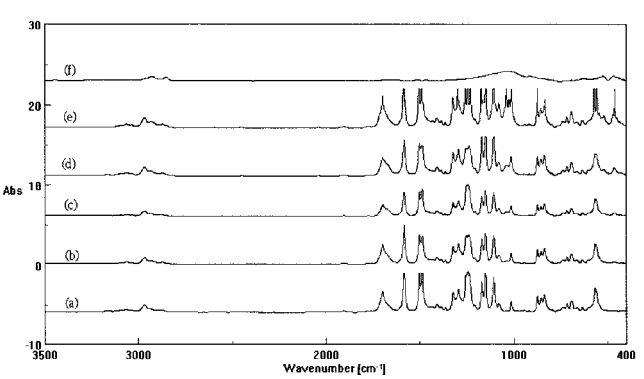

Figure 1 FTIR spectra of (a) PSF, (b) CLSF1, (c) CLSF5, (d) CLSF10 and (e) organophilic clay.

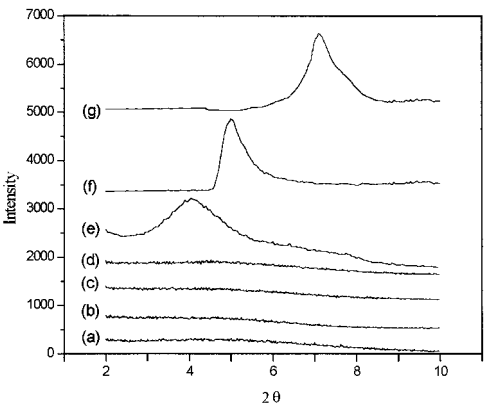

Figure 2 Wide-angle powder X-ray diffraction patterns of organophilic clay, PSF and a series of PSF–clay nanocomposite materials.

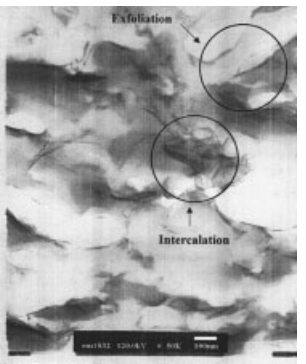

Figure 3 Transmission electron microscopy micrograph of CLSF10 at 50 K magnification.

corrosion potential (E_{corr}), polarization resistance (R_p), corrosion current (i_{corr}) and corrosion rate (R_{corr}), as listed in Table I. The CRS coupon coated with PSF showed a higher E_{corr} value than the uncoated CRS. However, it exhibited a lower E_{corr} value than the specimen coated with PCN materials. For example, the CLSF1-coated CRS had a high corrosion potential of approximately −529.7 mV at 30 min. Even after 5 h of measurement, the potential remained at about −535 mV. Such an E_{corr} value implies that the CLSF1-coated CRS is more corrosion-protected toward electrochemical corrosion than bulk PSF. The CLSF1-coated CRS showed a polarization resistance (R_p) value of 32.3 k°/cm^2 in 5 wt % NaCl, which is about 2 orders of magnitude greater than that of the uncoated CRS. The Tafel plots for uncoated, PSF-coated, CLSF1-coated and CLSF10-coated CRS are shown in Figure 4. For example, the corrosion current (i_{corr}) of CLSF1-coated CRS was about 1.7274 μA/cm^2, which corresponds to a corrosion rate (R_{corr}) of about 0.804 MPY. Electrochemical corrosion current values of PCN materials as coatings on CRS were found to decrease

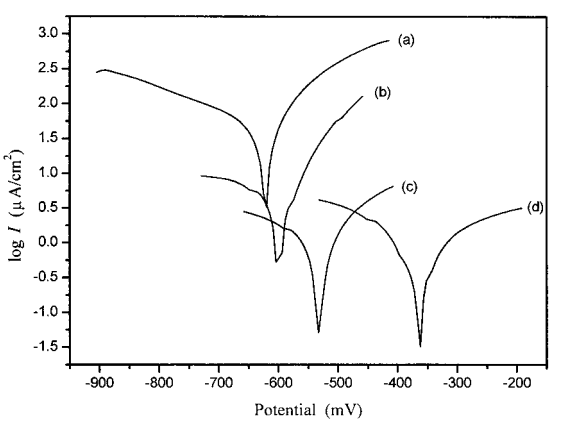

Figure 4 Tafel Plots for (a) uncoated, (b) PSF-coated, (c) CLSF1-coated and (d) CLSF10-coated CRS measured in 5 wt % NaCl aqueous solution.

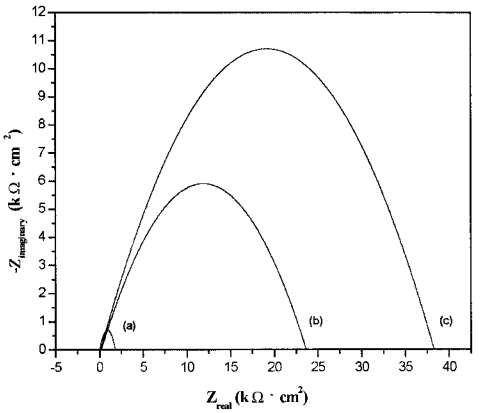

Figure 5 Nyquist plots for (a) uncoated, (b) PSF-coated and (c) CLSF1-coated CRS measured in 5 wt % aqueous NaCl solution.

gradually with further increase in clay loading. Electrochemical impedance spectroscopy (EIS) was also employed to evaluate the activity difference between CRS surfaces after PSF and PCN material treatment. Three samples were prepared. The first sample (a) was an uncoated CRS coupon. Samples (b-c) were coated with PSF and CLSF1. Figure 5 shows the Nyquist plots of the three samples. The charge transfer resistances of samples (a–c), as determined by the intersection of the low frequency end of the semicircle arc with the real axis, were 1.8, 23.7, 38.3 k°•cm^2, respectively. The results clearly demonstrate that the sample incorporating nanolayers of clay had the greatest anticorrosion performance. EIS Bode plots of the as-prepared materials are shown in Figure 6. The increase of impedance values at high clay loading in the low frequency range can be interpreted as the enhanced barrier effect of PCN materials when the nanolayers of MMT clay dispersed in the composites.

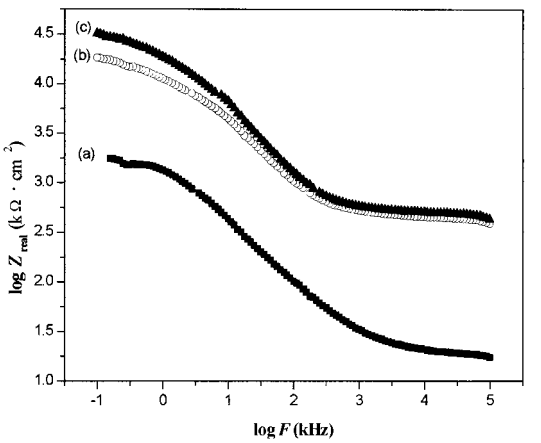

Figure 6 Bode plots for (a) uncoated, (b) PSF-coated and (c) CLSF1-coated CRS measured in 5 wt % aqueous NaCl solution.

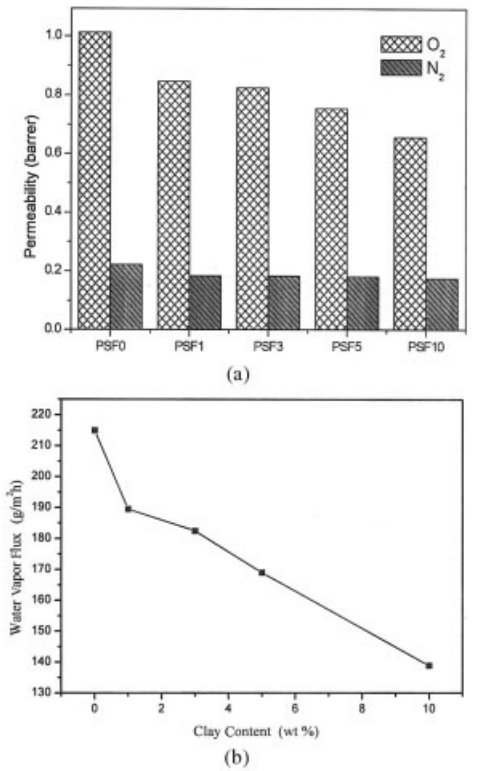

Figure 7 Permeability of (a) O_2/N_2 and (b) H_2O as a function of the MMT clay content in the PSF–clay nanocomposite materials.

Other Properties of Membranes

Gas Barrier Properties and Mechanical Strength of Membranes

Membranes of PCN materials and bulk PSF used for the molecular barrier measurements were prepared to have a film thickness of ≈50 μm. Compared to PSF, membranes of PCN materials at low clay loading (e.g. 3 wt %) showed about 30% and 72% reduction of H_2O and O_2 permeability, respectively, as shown in Figure 7. Furthermore, it should be noted that a further increase of clay loading resulted in a slightly enhanced molecular barrier property of bulk PCN materials. As shown in Figure 8, the storage modulus of PCN membranes with 3 wt % (E' = 1.187 × 10^8 Pa) and 10 wt % (E' = 2.332 × 10^8 Pa) clay loading [Fig. 8(b,c)] at room temperature (25°C) was found to be slightly higher than that of PSF (E' = 8.147 × 10^7 Pa) [Fig 8(a)]. This was attributed to the confinement of polymer chains by the presence of inorganic clay platelets in the polymeric matrix. There was found to be a major suppression in the storage modulus (E') starting around 120–130°C, which might be associated with the glass transition of PSF.

Optical Clarity of Membranes

Because of the nanoscale dispersion of the clays in the PSF matrix, optical clarity remained high at low clay contents (e.g. CLSF1), which yielded primarily exfoliated composites.[23,24] Figure 9 shows the UV-visible transmission spectra of bulk PSF and PSF–clay nanocomposites with 1 wt %, 5 wt % and 10 wt % MMT. These membranes had a thickness of ≈30 μm. The spectra of CLSF1 show that the visible region (400–700 nm) was almost unaffected by the presence of clay and retained the high transparency of the PSF. However, the spectra of CLSF5 and CLSF10, which exhibited low transparency of the PSF, reflected the primarily intercalated composites. For the ultraviolet wavelength, there was strong scattering and/or absorption, resulting in very low transmission of UV light.

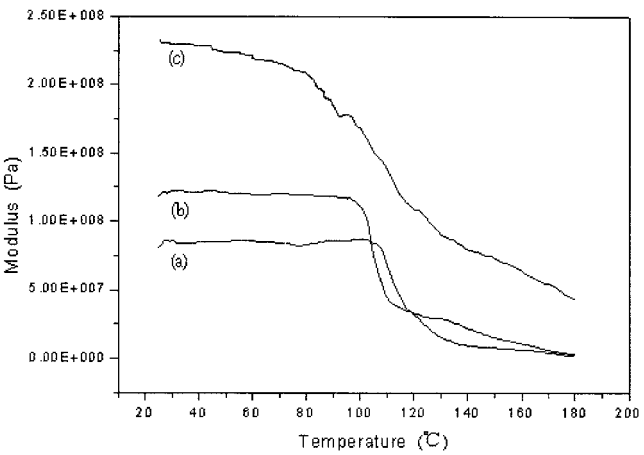

Figure 8 DMA curves of (a) PSF, (b) CLSF3 and (c) CLSF10.

CONCLUSIONS

A series of PCN materials was prepared by effectively dispersing inorganic nanolayers of MMT clay in organic PSF matrix via a solution dispersion technique. The as-synthesized PCN materials were characterized by FTIR spectroscopy, wide-angle powder X-ray diffraction (XRD) and TEM. PCN coatings with low clay loading (e.g. 1 wt %) on CRS were found to be superior in anticorrosion properties

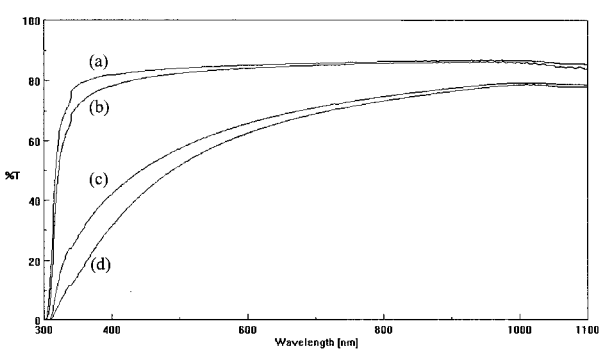

Figure 9 UV-visible transmission spectra of (a) PSF, (b) CLSF1, (c) CLSF5 and (d) CLSF10.

over those of bulk PSF, based on a series of electrochemical measurements of corrosion potential, polarization resistance, corrosion current and impedance spectroscopy in a 5 wt % aqueous NaCl electrolyte. The enhanced anticorrosion of PSF–clay nanocomposite materials compared to bulk PSF might be a result of dispersing silicate nanolayers of clay in the PSF matrix to increase the tortousity of the diffusion pathway of oxygen and water. The effects of the material composition on the molecular barrier, mechanical strength and optical clarity of PSF along with PCN materials, in the form of membranes, was also studied by molecular permeability analysis (GPA), dynamic mechanical analyzer (DMA) and UV-visible transmission spectra, respectively. The membranes of PCN materials at low clay loading (e.g. 3 wt %) compared to PSF were found to show about 30% and 72% reduction in H_2O and O_2 permeability, respectively. The incorporation of clay into the PSF matrix led to an increase in storage modulus compared to bulk PSF membrane. The UV-transmission spectra of nanocomposite membranes at low clay loading (e.g. 1 wt %) showed that the visible region (400–700 nm) was almost unaffected by the presence of the clay and retained the high transparency of the PSF.

The financial support of this research by the NSC 90-2113-M-033-010 is gratefully acknowledged.

References

1. Giannelis, E. P. J Min, Met & Mat Soc 1992, March, 28.
2. Jordan, J. M. J Phys Colloid Chem 1950, 53, 245.
3. Lan, T.; Kaviratna, P. D.; Pinnavaia, T. J. Chem Mater 1994, 6, 573.
4. Tyan, H.-L.; Liu, Y.-C.; Wei, K.-H. Chem Mater 1999, 11, 1942.
5. Wang, Z.; Pinnavaia, T. J. Chem Mater 1998, 10, 3769.
6. Gilman, J. W.; Jackson, C. L.; Morgan, A. B.; Hayyis, Jr. R.; Manias, E.; Giannelis, E. P.; Wuthenow, M.; Hilton, D.; Phillips, S. H. Chem Mater 2000, 12, 1866.
7. Usuki, A.; Kawasumi, M.; Kojima, Y.; Okada, A.; Karauchi, T.; Kamigaito, O. J Mater Res 1993, 8, 1774.
8. Choi, Y. S.; Wang, K. H.; Xu, M.; Chung, I. J. Chem Mater 2002, 14, 2936.
9. Lee, D. C.; Jang, L. W. J Appl Polym Sci 1996, 61, 1117.
10. Akelah, A.; Rehab, A.; Selim, A.; Agag, T. J Mol Catal 1994, 94, 311.
11. Agag, T.; Koga, T.; Takeichi, T. Polymer 2001, 42, 3399.
12. Lee, D. C.; Jang, L. W. J Appl Polym Sci 1998, 68, 1997.
13. Wang, Z.; Pinnavaia, T. J. Chem Mater 1998, 10, 3769.
14. Dai, L.; Wang, Q.; Wan, M. J Mater Sci Lett 2000, 19, 1645.
15. Biswas, M.; Ray, S. S. Polymer 1998, 39, 6423.
16. Wang, L.; Brazis, P.; Rocci, M.; Kannewurf, C. R.; Kanatzidis, M. G. In Organic/Inorganic Hybrid Materials; Laine, R. M., Sanchez, C., Brinker, J. F., Giannelis, E., Eds. Materials Research Society: Warrendale, PA, 1998; vol.519, p 257.
17. Yeh, J.-M.; Liou, S.-J.; Lai,C.-Y.; Wu, P.-C.; Tsai, T.-Y. Chem Mater 2001, 13, 1131.
18. Yeh, J.-M.; Liou, S.-J.; Lin, C.-Y.; Cheng, C.-Y.; Chang, Y.-W. Chem Mater 2002, 14, 154.
19. Yeh, J.-M.; Chen, C.-L.; Chen, Y.-C.; Ma, C.-Y.; Lee, K.-R.; Wei, Y.; Li, S. Polymer 2002, 43, 2729.
20. Stevens, M. P. In Polymer Chemistry: An Introduction, 3rd ed.; Oxford University Press: Oxford, 1999; p 311.
21. Sur, G. S.; Sun, H. L.; Lyu, S. G.; Mark, J. E. Polymer 2001, 42, 9783.
22. Yano, K.; Usuki, A.; Okada, A. J Polym Sci, Polym Chem Ed 1997, 35, 2289.
23. Wu, C.-G.; DeGroot, D. C.; Marcy, H. O.; Schindler, J. L.; Kannewurf, C. R.; Liu, Y.-J.; Hirpo, W.; Kanatzidis, M. G. Chem Mater 1996, 8, 1992.
24. Strawhecker, K. E.; Manias, E. Chem Mater 2000, 12, 2943.